PHYSICAL REVIEW B **96**, 035103 (2017)

Ab initio prediction of the high-pressure phase diagram of $BaBiO_3$

Andriy Smolyanyuk,[1] Lilia Boeri,[1] and Cesare Franchini[2]
[1]*Institute of Theoretical and Computational Physics, Graz University of Technology, NAWI Graz, 8010 Graz, Austria*
[2]*Faculty of Physics, University of Vienna, 1090 Vienna, Austria*

(Received 15 February 2017; revised manuscript received 2 May 2017; published 5 July 2017)

$BaBiO_3$ is a well-known example of a 3D charge density wave (CDW) compound, in which the CDW behavior is induced by charge disproportionation at the Bi site. At ambient pressure, this compound is a charge-ordered insulator, but little is known about its high-pressure behavior. In this work, we study from first principles the high-pressure phase diagram of $BaBiO_3$ using phonon mode analysis and evolutionary crystal structure prediction. We show that charge disproportionation is very robust in this compound and persists up to 100 GPa. This causes the system to remain insulating up to the highest pressure we studied.

DOI: 10.1103/PhysRevB.96.035103

I. INTRODUCTION

Transition-metal oxide perovskites are currently a subject of intense study, since they exhibit many interesting properties which make them attractive for both fundamental and applied research. Ferroelectricity [1], high-T_c superconductivity, charge ordering, and colossal magnetoresistance [2] are some of the most intriguing examples. One of the most distinctive materials of this family is $BaBiO_3$ [3,4], which is a charge-ordered insulator and becomes superconducting upon doping [5,6].

Recent studies have shown that also at reduced dimensionality $BaBiO_3$ exhibits several remarkable properties: experimental investigation of suppression of structural distortion in thin films [7] and suppression of the charge density wave (CDW) in the $BaBiO_3$ films [8], as well as theoretical predictions of topological phases [9] and 2D electron gas at the surface [10], were recently reported in the literature.

In this compound Bi behaves as a mixed-valence element and can occur in either the formal Bi^{3+} or Bi^{5+} oxidation state. The $BaBiO_3$ compound can thus be seen as an $ABB'O$ perovskite where B is Bi^{3+} and B' is Bi^{5+}. Although the Bi^{4+} oxidation state was never observed in any other compounds, a hypothetical $BaBi^{4+}O_3$ should have an ideal perovskite cubic—$Pm\bar{3}m$—structure [Fig. 1(a)] and should be a metal. The mixed valence state of Bi and the periodical arrangement of atoms leads to formation of a CDW state. This has two consequences: the different attraction strength of oxygen to the two types of Bi leads to a chess-pattern breathing distortion of the Bi-O octahedra; in turn, this CDW breathing distortion splits the antibonding Bi(s)-O(p) antibonding state and establishes an insulating ground state [11,12].

Upon hole doping $BaBiO_3$ undergoes an insulator to metal transition and becomes a superconductor; superconducting T_c's up to 13 K were reported for $BaPb_{1-x}Bi_xO_3$ [5], and up to 34 K for $Ba_{1-x}K_xBiO_3$ [6]. The suppression of the CDW state upon doping, and the occurrence of superconductivity, have been intensely debated in the literature [11–21]. Only recently, with the adoption of post-DFT techniques, it has been possible to obtain a consistent description of the whole phase diagram.

In many compounds, high pressure is a viable alternative to doping to tune the material properties. In particular, this has recently been exploited in several 2D transition-metal dichalcogenides to study the interplay of CDW and superconductivity. For instance, it was demonstrated that in pristine 1T-$TiSe_2$ [22] and 2H-$NbSe_2$ [23] pressure induces a quantum melting of the CDW. It is extremely intriguing to investigate whether a similar behavior could occur in $BaBiO_3$, i.e., whether pressure could be used to suppress the three-dimensional CDW insulating state and promote a metallic, superconducting state. Based on simple theoretical arguments, all insulators should become metallic at high enough pressure (or density), due to increasing hybridization and higher bandwidth. It is reasonable therefore to expect that, under pressure, $BaBiO_3$ should undergo a structural transition to the ideal perovskite structure, becoming metallic by band overlap. However, this picture may be too naive.

In fact, in the last two decades the study of matter at extreme conditions has shown that even simple elements exhibit a physical and chemical behavior, which cannot be explained in these simple terms. For instance, simple free-electron metals such as lithium and sodium become insulating under pressure [24,25]; hydrides, which form insulating molecular crystals at ambient pressure, can become metallic, and exhibit superconductivity with T_c's as high as 200 K [26–36]; even higher T_c's have been predicted for elemental hydrogen, above the Wigner-Huntington transition [37–40]. Explaining the high-pressure behavior of solids thus requires first an accurate understanding of the structural modifications induced by pressure.

The aim of this work is to investigate the possibility of suppressing the CDW state and induce an insulator to metal transition in $BaBiO_3$ under pressure, performing a theoretical study of its crystal and electronic structure. Since the available experimental information is extremely limited, we are using two structural prediction techniques to determine the possible high-pressure phases. The first is based on group-theoretical analysis of irreducible representations of unstable phonon modes using the ISOTROPY software suite [41,42] and the second is based on using evolutionary algorithm approaches as implemented in the USPEX package [43].

The first is a classic, elegant approach which is able to describe the most typical structural distortions occurring in transition-metal perovskites. The basic idea is that continuous phase transitions may be classified using group-subgroup relations where the distorted phase is described by a subgroup of the space group of the parent phase. Subgroups which

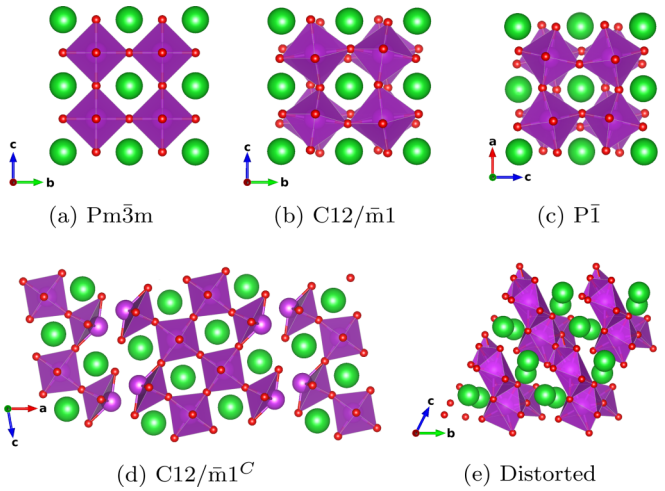

FIG. 1. $BaBiO_3$ ground-state structures used in this work. (a) $Pm\bar{3}m$: ideal perovskite structure. (b) $C12/\bar{m}1$: experimental $BaBiO_3$ structure for ambient pressure and room temperature. (c) $P\bar{1}$: triclinic structure stable from 20 GPa to 28 GPa pressure. (d) $C12/\bar{m}1^C$: *clustered* monoclinic structure stable between 28 GPa and 87 GPa pressure. (e) Nonsymmetric *distorted* structure stable from 87 GPa pressure. Structures (c), (d), and (e) where obtained using evolutionary crystal structure prediction (EP). Large green spheres are Ba atoms, large purple spheres are Bi atoms, and small red spheres are O atoms.

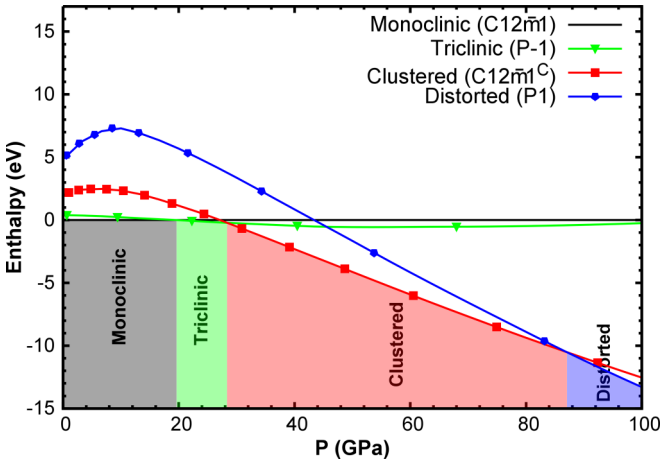

FIG. 2. Predicted high-pressure phase diagram of $BaBiO_3$. Up to 100 GPa, we predict three structural phase transitions: monoclinic ($C12\bar{m}1$) to triclinic ($P\bar{1}$) at about 20 GPa, triclinic to clustered ($C12\bar{m}1^C$) at about 28 GPa, and clustered to distorted ($P1$) at about 87 GPa. The values of the enthalpies are referred to a 40 atoms unit cell.

consist of operations that leave the order parameter invariant are called *isotropy* subgroups and they may be deduced from irreducible representations of the parent group [44]. The ISOTROPY software suite provides a convenient tool for the group-theoretical analysis of phase transitions in solids based on the theory of isotropy subgroups. In our case, we further refined the subset of subgroups of the ideal perovskite structures performing an analysis of the eigenvectors of the phonon modes that become unstable at different pressures, as described in detail in Sec. II B. The second is a more general approach to the prediction of crystal structures, inspired by biological evolution. The idea is to generate and evolve a *population* of crystal structures, applying various variation operators which are similar to biological mechanisms such as reproduction, mutation, recombination, and selection to minimize a fitness function, which is typically the enthalpy of the system, obtained from an accurate *ab initio* calculation. Evolutionary algorithms have been proven very successful at predicting the crystal structure of actual materials in many cases [43]. In contrast to the previous method, in this case the set of possible structures is not limited to a subgroup of the perovskite structure, but is completely general. Further details can be found in Sec. II C.

Our calculations based on the two approaches above show that charge ordering persists up to 100 GPa and the system remains insulating in this pressure range.

To investigate the electronic properties we are using a hybrid Hartree-Fock/density functional theory (DFT) calculation with the HSE (Heyd-Scuseria-Ernzerhof) exchange-correlation functional [45]. In fact, the role of electronic correlations on the accurate description of the CDW was discussed in many papers and it was shown that it is essential to use post-DFT approaches to obtain a proper description of the electronic structure of this system [11,18,19,21].

This paper is organized as follows: In Sec. II we describe the results of our *ab initio* calculations starting with our prediction for the high-pressure phase diagram (Sec. II A), followed by the description of the phonon mode analysis in Sec. II B. We present the results obtained with the *ab initio* evolutionary prediction method in Sec. II C and electronic properties of the predicted ground-state structures are analyzed in Sec. II D. The main conclusions of this work are summarized in Sec. III. Computational details are described at the end of the paper in Sec. IV.

II. RESULTS

$BaBiO_3$ was synthesized for the first time in 1963 [46] and was identified as a perovskite but it was hard to precisely determine the right structure: rhombohedral, orthorhombic, monoclinic, or triclinic symmetries were reported by various groups [3,47,48]. It was finally established that at room temperature and ambient pressure the structure is monoclinic ($C12\bar{m}1$), Fig. 1(b). This structure can be described as a perovskite with two types of distortions: *breathing* and *tilting* distortions of Bi-O octahedra. In the breathing distortion the octahedra alternate in size, while upon tilting the octahedra are rotated. The role of the breathing and tilting distortions has been widely discussed in the literature. In particular, DFT calculations reported conflicting results [13–16]. Only recently the use of post-DFT methods has permitted us to reproduce the experimental findings correctly [11,18,19].

A. Predicted phase diagram

Figure 2 shows our predicted high-pressure phase diagram [49]. The system undergoes three structural phase transitions and remains insulating up to 100 GPa. Figure 1 shows the structures which are most relevant

for the discussion (the structures are provided as CIF files in the Supplemental Material [50]). An extended version of the phase diagram is provided in Fig. 1 of the Supplemental Material [51].

As a reference structure we chose the monoclinic ($C12\bar{m}1$) $BaBiO_3$ structure, which was determined by the experiment at ambient pressure. The structures with *EP* after the title are the best structures obtained using the evolutionary crystal structure prediction method. They become energetically favorable in the high-pressure region. The structures with *SA* are obtained using the group-theoretical approach for crystal structure prediction. At high pressure these structures are energetically more favorable than our reference ($C12\bar{m}1$) structure, but are way behind the structures obtained using the evolutionary method. The *P-Perovskite* is a post-perovskite structure that we added into consideration by chemical intuition. This structure was obtained by Oganov *et al.* for $MgSiO_3$ at extreme pressure and has 20 atoms in the unit cell [52].

Following the lowest enthalpy path in our calculated phase diagram, we find that a first transition from the monoclinic [$C12\bar{m}1$, see Fig. 1(b), 10 atoms in the unit cell] to triclinic [$P\bar{1}$, see Fig. 1(c), 40 atoms in the unit cell] structure occurs at about 20 GPa. The $P\bar{1}$ structure is a distortion of the $C12\bar{m}1$ structure with one additional tilting axis. A transition from triclinic ($P\bar{1}$) to clustered monoclinic [$C12\bar{m}1^C$, Fig. 1(d), 40 atoms in the unit cell] occurs at about 28 GPa. We call this structure *clustered* because it has "domains" created by shearing parts of the original structure. The last transition is at about 87 GPa, where the clustered monoclinic ($C12\bar{m}1^C$) is transformed to a highly distorted structure with no symmetry [$P1$, see Fig. 1(e), 20 atoms in the unit cell]. We will refer in text to it as *distorted*.

The experimental information about $BaBiO_3$ at high pressure is extremely scarce and limited to $P \leqslant 20$ GPa [53,54]. Unfortunately, the experimental resolution was not enough to have a full refinement of the crystal structure. An anomaly at about 4 GPa was reported, at which the bulk modulus decreases and this was attributed to the change of the tilt system (due to additional type of octahedra tilting). Moreover it was reported that the system remains insulating up to at least 10 GPa. Our results are consistent with the measurements that $BaBiO_3$ is an insulator in this pressure range. However, we cannot reproduce the anomaly at 4 GPa.

Before discussing in detail the crystal and electronic structure across the phase diagram, we will illustrate the details of our structural search methods.

B. Phonon mode analysis

The group-theoretical method has been successfully used to identify and predict structural distortions in a variety of perovskites [55,56]. A powerful extension is to combine this method with the results of a phonon mode analysis of the parent structure [57]. For $BaBiO_3$ the starting point is the ideal cubic perovskite structure, Fig. 1(a). It has a $P3\bar{m}3$ (cubic) symmetry with 5 atoms in the unit cell; it is a metal, since no charge disproportionation is possible in this case. The six O nearest neighbors of Bi form a perfect octahedron. This octahedron can be distorted in several ways and there are two

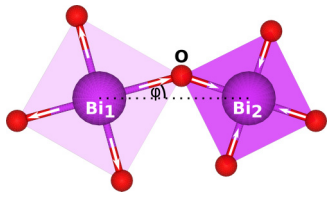

FIG. 3. Breathing and tilting distortions applied to an ideal cubic perovskite structure. Breathing is indicated by squares of different size where the white arrows show the direction in which O atoms are displaced. Tilting is shown as a rotation of a square by angle φ around axis normal to the plane of the paper.

kinds of distortions usually present in real perovskite systems: *breathing* and *tilting* (see Fig. 3).

A *breathing* distortion means that some O atoms move closer or farther away from the Bi atom, which is located at the center of the octahedron. Octahedra are coupled to each other and the breathing of one of them creates an opposite breathing on its neighbors. There are different kinds of breathing distortions depending on which and how many pairs of O are distorted. In the monoclinic structure of $BaBiO_3$ all O atoms are involved in the breathing distortion and the overall picture is a 3D chess pattern of octahedra with alternating sizes. A *tilting* distortion is the rotation of an octahedron around a tilting axis. Neighboring octahedra in the plane normal to the tilting axis are coupled and rotate in the opposite direction. Octahedra in adjacent planes may rotate in the same (*in-phase* rotation) or in the opposite direction (*antiphase* rotation). The latter is present in monoclinic $BaBiO_3$.

The ideal cubic perovskite is dynamically unstable at ambient pressure and room temperature, and the analysis of unstable phonon modes gives an insight of which distortions correspond to a lowering of the energy of the system and thus allow us to predict more favorable structures. This can be achieved by computing the phonon dispersion relations and the corresponding eigenvectors. Eigenvectors with imaginary eigenvalues represent the direction of atomic displacements that lead to a decrease in energy. The stable structure can then be obtained following the most favorable distortion, which may be a linear combination of unstable phonon eigenvectors. The space of possible combinations can be reduced using the group-theoretical method and the unstable phonon modes mapping on the corresponding irreducible representations.

We calculated the phonon dispersion relations and the corresponding phonon eigenvectors for $BaBiO_3$ in the ideal cubic perovskite structure using a finite-difference supercell method [58,59], and classified unstable eigenvectors with the corresponding irreducible representations. We first tested our approach at ambient pressure, and the results we obtained are consistent with the experimental structure (see below). After that, the investigation of stability of modes was repeated for several pressures in the range from 0 to 100 GPa (see Fig. 2 of the Supplemental Material [60]); the results for 0 GPa and 100 GPa pressure are summarized in Table I.

At ambient pressure our result is consistent with the experimentally reported structure, namely monoclinic $BaBiO_3$, since this structure can be obtained combining a breathing distortion with irreducible representation R1+ and the R4+ irre-

TABLE I. Irreducible representations associated with unstable phonon eigenvectors of the $P3\bar{m}3$ structure at 0 GPa and 100 GPa pressure. "#" is the mode number.

	P=0 GPa		P=100 GPa			
#	M	R	Γ	M	R	X
1	M3+	R1+	Γ4-	M3+	R4+	X5-
2		R4+		M5-		
3						
4			Γ5-	M3-		
5						
6						

ducible representation tilting ($a^0b^-b^-$ in Glazer notation [61]) distortion, which are both present in the results of our analysis. The M3+ irreducible representation is an in-plane breathing distortion, which is not present in monoclinic $BaBiO_3$ because the R1+ breathing is more favorable.

In Table II we report the values of the breathing distortion (δ), the tilting angle (φ), and equilibrium volume (V_0) for the ambient pressure structure measured by experiment and calculated using both the PBE (Perdew-Burke-Ernzerhof) exchange-correlation functional in the anzatz of the generalized gradient approximation (GGA) and HSE functionals. HSE gives a more accurate description of the structure, and reproduces correctly the electronic properties: monoclinic $BaBiO_3$ is a charge-ordered insulator with a band gap of about 0.8 eV, while in GGA it is a zero-gap semiconductor. Although our calculations predict a transition from the monoclinic to the triclinic structure already at around 20 GPa, we followed the evolution of the monoclinic structure to high pressure to see whether the monoclinic distortions are suppressed. We find that the distortions are preserved under pressure and the tilting angle φ is proportional to pressure. Thus, the CDW is very robust in this compound and is not suppressed under pressure. Up to about 85 GPa the band gap increases but afterwards its value decreases and the structure becomes a semimetal (the related information is provided in Fig. 3 of the Supplemental Material [62]).

TABLE II. List of calculated by PBE and HSE values for monoclinic ($C12\bar{m}1$) structure in comparison with experimental data. δ is breathing distortion [$\delta = \frac{1}{2}(\overline{Bi_1O} - \overline{Bi_2O})$, where $\overline{Bi_1O}$ and $\overline{Bi_2O}$ are average Bi_1-O and Bi_2-O bond distances, respectively], φ is the average tilting angle, and V is the volume per one formula unit of $BaBiO_3$.

	δ (Å)	φ (deg)	V_0 (Å^3)
PBE	0.074	11.97	85.92
HSE	0.096	10.95	82.67
PBE [18]	0.07	12.1	85.76
HSE [18]	0.09	11.9	82.10
Experiment [3]	0.09	10.1	82.11

There are two regions were a substantial change in stability of the phonon modes takes place: at about 30 GPa the R1+ mode become stable and at about 70 GPa the M3− and M5− modes become unstable (for details see Fig. 2 of the Supplemental Material [60]). Based on the eigenvector analysis at 100 GPa, we constructed a pool of candidate high-pressure structures. This pool is valid also at lower pressures, since unstable modes at lower pressures are a subset of the 100 GPa ones. In particular, we have used the M3+, M5−, and R4+ irreducible representations. In total, we investigated 17 structures with 10, 20, and 40 atoms in the unit cell (see Table V of the Supplemental Material for irreducible representations and order parameters used to obtain these structures [63]). The structures $P4\bar{m}bm$, $I4\bar{m}bm$, and $I4\bar{m}bm^B$ (see Fig. 1 of the Supplemental Material [51]) are the best obtained by this method followed by DFT relaxations. $P4\bar{m}bm$ is obtained from the ideal perovskite structure by applying in-phase tilting ($a^0a^0c^+$ in Glazer notation [61]) and $I4\bar{m}bm$ by antiphase tilting ($a^0a^0c^-$). $I4\bar{m}bm^B$ is equivalent to $I4\bar{m}bm$ with an additional in-plane breathing distortion. These three structures are metals, but they are around 7 to 13.5 eV higher in enthalpy with respect to the ground state at 100 GPa, and thus very unlikely to be observed in experiments.

C. *Ab initio* evolutionary prediction

We performed *ab initio* evolutionary algorithm calculations at fixed composition for structures with 10, 20, and 40 atoms in the unit cell corresponding to 2, 4, and 8 formula units (f.u.) respectively. The 10-atom 0 GPa calculation was used to test the reliability of the method. The structure we obtained for this run is consistent with the experiment. Calculations with 10, 20, and 40 atoms were made at 50 and 100 GPa. Up to 5–10 best structures from each run were chosen for more accurate relaxations to obtain the final ranking of the energies and were relaxed for various pressures in the pressure range from 0 to 100 GPa using fixed-volume relaxation allowing cell shape to change but with the symmetry fixed to obtain the equation of state.

The analysis of phonon modes for the monoclinic structure indicates a possible structural transition in the range of 25–30 GPa. To check this region more carefully we performed additional calculations at 25 GPa for structures with 20 and 40 atoms in the unit cell, and 30 GPa for structures with 10 atoms in the unit cell. As a result, we found a triclinic $P\bar{1}$ structure that is stable in the 20–28 GPa pressure region [Fig. 1(c)]. As already mentioned, the evolutionary algorithm approach was able to find the structures that are the energetically most stable ones at high pressures (i.e., more stable than the best SA ones). These are triclinic ($P\bar{1}$), clustered ($C12\bar{m}1^C$), and distorted ($P1$). There are both metals and insulators present in the pool of all structures obtained by these structural search calculations, but the most energetically favorable are always insulating and strongly disordered.

The evolutionary algorithm calculations thus show that $BaBiO_3$ has a tendency to become more distorted when pressure is increased, destabilizing the perovskite environment without suppressing the charge disproportionation. In order to understand this tendency, we have performed an additional analysis, measuring the change in the bonding environment of Bi in terms of its average number of neighbors [64–67].

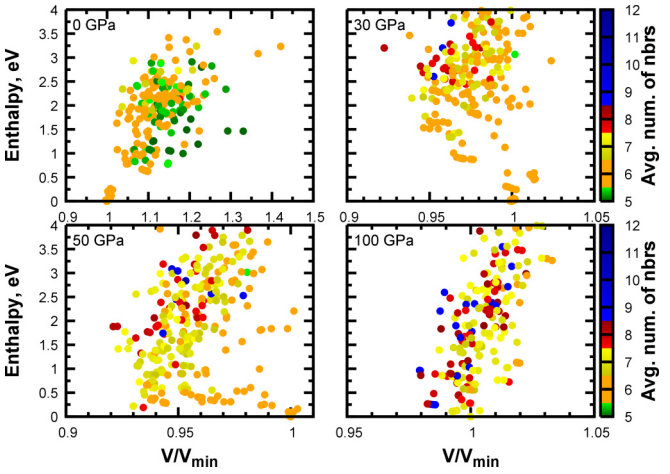

FIG. 4. Average number of O neighbors of Bi atoms for a pool of 2 f.u. $BaBiO_3$ structures obtained using the evolutionary algorithms approach. Each dot is associated with a specific structure and its color denotes the average number of neighbors. For the perovskite structure the average number of neighbors is 6 and the deviation from this value shows the amplitude of distortion presented in the system. Details on the neighbor analysis can be found in the Supplemental Material in subsection "D. Neighbors analysis" [68].

In an ideal perovskite this number is six; significant deviations from this value indicate strong distortions. The result of this analysis is presented in Fig. 4 (for details see the subsection "D. Neighbors analysis" of the Supplemental Material [68]). In Fig. 4 each structure at the corresponding pressure is represented by a dot, with the color indicating the average number of neighbors of Bi and the coordinates describing the volume and enthalpy of the structure. The volume is rescaled to the volume of the ground-state structure for a given pressure ($V_{\min}$) and the enthalpy is given with respect to the enthalpy of the ground-state structure. As expected, at ambient pressure for the low-enthalpy structures there are six O atoms in the Bi environment, while with increasing pressures structures with seven or more neighbors become competitive and finally become the ground-state ones. The plot thus shows that there is a general trend for $BaBiO_3$ to break the perovskite structure and become more distorted.

Note that in order to maintain a reasonable computational cost, we performed this analysis using the results of the structural search for 2 f.u. structures, under the assumption that the tendency to distortion should be so general to show up already for smaller structures. In order to check the validity of this assumption, we cross-checked our results for a single pressure (100 GPa) for 8 f.u. structures, and found that, indeed, our assumption is correct, as also in this case low-lying structures have an average number of neighbors significantly larger than six.

D. Electronic properties

We analyzed the electronic properties of all four ground-state structures using both PBE and HSE functionals. Our calculations show that all structures are insulating (see Fig. 5); the tendency is to become more insulating with increasing pressure. Only the $C12\bar{m}1^C$ structure is metallic at the PBE

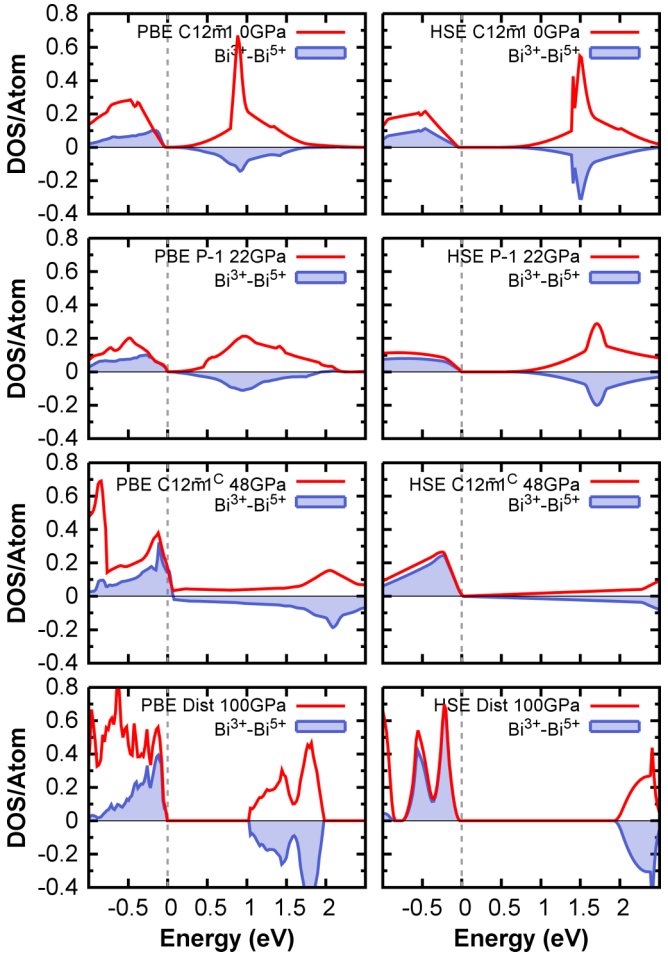

FIG. 5. DOS/atom and the difference of average PDOS for Bi^{5+} and Bi^{3+} atoms [69] for stable structures at the pressure of its stability. Left panel shows results obtained with PBE functional for structural relations and DOS calculations. Right panel shows results for structures at the left panel but DOS calculations were performed using the HSE functional using the structures from PBE calculations.

level but on the HSE level opens a gap [70]. Here the use of the HSE functional is important as PBE underestimates the band gap or predicts the structure to be a metal while actually it is an insulator [18]. Analyzing the partial DOS for Bi atoms it can be seen that all the structures have two inequivalent Bi atoms with different formal valence state, and the insulating behavior is associated with the CDW. In particular, the empty states have a dominant Bi^{5+} character, while the valence band is essentially formed by Bi^{3+} states, which have a strong hybridization with Op states. As a consequence, the total DOS essentially coincides with the partial Bi DOS for the empty states, but not for the valence band.

We determine the magnitude of the charge disproportionation by calculating the charge difference $\Delta\rho$ for the two types of bismuth, Bi^{3+} and Bi^{5+}, from the partial *spd* charge of the site-projected ground-state wave function; see Fig. 6. Note that although we name these atoms Bi^{3+} and Bi^{5+}, the actual difference in charge is much smaller than two [18].

For the $C12\bar{m}1$, $P\bar{1}$, and $C12\bar{m}1^C$ structures the charge disproportionation increases when the pressure is increased.

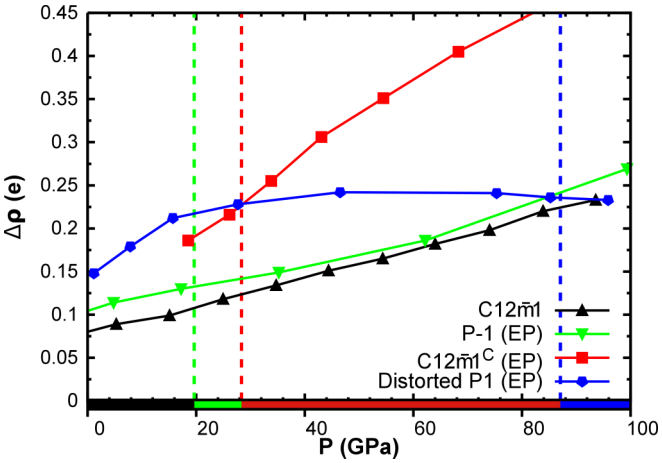

FIG. 6. Charge difference $\Delta\rho$ between two different Bi atoms for all stable structures in the phase diagram: the one with the maximal charge (represented by the Bi^{3+} atom) and the one with the minimal (represented by the Bi^{5+} atom); the HSE functional was used. The color scale at the bottom indicates the stability range of the various structures.

The change of charge disproportionation for the distorted structure in the pressure range from 20 GPa to 100 GPa is small.

The only possible way to suppress the CDW and have a metallic $BaBiO_3$ phase is to have a highly symmetric structure with no inequivalent Bi atoms as electronic properties of $BaBiO_3$ are highly coupled to the structural ones. Our calculations show that for $BaBiO_3$ all energetically favorable structures are distorted in such a way that they are forced to be insulators, and metallic (symmetric) structures are strongly unfavorable in energy, and thus very unlikely to occur.

III. CONCLUSIONS

In this work we performed a theoretical study of the $BaBiO_3$ phase diagram under pressure to analyze the possibility of suppressing the CDW distortion, caused by charge disproportionation. We used two different structural search approaches to construct our *ab initio* predicted high-pressure phase diagram: evolutionary algorithms and phonon mode analysis. The resulting phase diagram shows three structural phase transitions. The group-theoretical structure prediction method alone, which has been successfully applied to describe the structure of many transition-metal perovskites, is not able to find the best structures at high pressure as it is constrained only to structures with symmetry. By using evolutionary algorithms we found that $BaBiO_3$ becomes more distorted with increasing pressure. In fact, our calculations show that high pressure favors complicated structures with clustering and shearing distortions, which cannot be described as symmetry distortions of the single perovskite structures. The analysis of the electronic properties show that all ground-state structures remain insulating up to 100 GPa and the charge disproportionation is preserved at high pressure. This hinders the transition towards a metallic regime.

IV. COMPUTATIONAL DETAILS

For total energies and structural optimization we used GGA and HSE DFT calculations, as implemented in the VASP package [72–75] using PAW pseudopotentials [76,77]. We used the hybrid HSE functional to improve the description of the electronic properties. The energy cutoff value was set to 500 eV and a Γ-centered Monkhorst-Pack grid [78,79] with $4 \times 4 \times 4$ k points was used for the GGA [80,81] and HSE functional for the structural relaxation. To do the relaxation at a specific pressure we performed fixed-volume calculation. For DOS calculations we used an $8 \times 8 \times 8$ grid for the GGA functional and a $2 \times 2 \times 2$ for HSE which was sufficient to converge the value of the semiconducting gap (note that all structures at the HSE level are semiconducting). Phonon calculations were done with a $20 \times 20 \times 20$ k-point grid at the PBE level with a $2 \times 2 \times 2$ supercell.

We have used two approaches to predict possible structures at high pressure: evolutionary algorithms as implemented in the USPEX package [43] and the group-theoretical analysis using the ISOTROPY software suite [41]. Determination of dispersion relations was done with the PHONOPY package [58]. The setup for USPEX calculations was the following: 20 structures in population, 40 structures in the initial population, maximal number of generations is 25, and we stopped the search when the best structure did not change for 8 generations.

The analysis of the Bi environment for the pool of structures obtain in the USPEX calculations was performed using the CHEMENV module from the PYMATGEN package [64–66]. The main goal of the CHEMENV module is to determine the chemical environment of each atom in a structure finding the best polyhedron that can represent atomic positions using *continuous symmetry measure* as a parameter to determine the optimal polyhedron (more details can be found in the Supplemental Material [82]). The pool of structures consists of around 300 structures for each pressure with 10 atoms in the unit cell.

Note added. Recently we became aware of a joint theoretical and experimental study by Martoňák *et al.* [71] on the high-pressure phase diagram of $BaBiO_3$. The resistivity data confirm our prediction that $BaBiO_3$ remains insulating up to at least 80 GPa. The authors also report a theoretical phase diagram in excellent agreement with ours, confirming our main conclusion that $BaBiO_3$ remains a charge-ordered insulator up to high pressures, forming more and more distorted structures.

ACKNOWLEDGMENTS

We thank Jiangang He for useful discussions and helpful instructions on symmetry analysis and David Waroquiers and Geoffroy Hautiers for the development of the CHEMENV package and very helpful technical support on its use. We acknowledge funding from the Austrian Science Fund FWF through SFB ViCoM, Project F41-N28-P15, and computational resources from the VSC3 of the Vienna University of Technology. We are also grateful to Erio Tosatti for pointing out to us Ref. [71].

[1] R. E. Cohen, Nature (London) **358**, 136 (1992).
[2] B. Raveau, A. Maignan, C. Martin, and M. Hervieu, Chem. Mater. **10**, 2641 (1998).
[3] D. Cox and A. Sleight, Solid State Commun. **19**, 969 (1976).
[4] A. W. Sleight, Phys. C (Amsterdam, Neth.) **514**, 152 (2015).
[5] S. Uchida, K. Kitazawa, and S. Tanaka, Phase Transitions **8**, 95 (1987).
[6] R. J. Cava, B. Batlogg, J. J. Krajewski, R. Farrow, L. W. Rupp, A. E. White, K. Short, W. F. Peck, and T. Kometani, Nature (London) **332**, 814 (1988).
[7] K. Inumaru, H. Miyata, and S. Yamanaka, Phys. Rev. B **78**, 132507 (2008).
[8] G. Kim, M. Neumann, M. Kim, M. D. Le, T. D. Kang, and T W. Noh, Phys. Rev. Lett. **115**, 226402 (2015).
[9] B. Yan, M. Jansen, and C. Felser, Nat. Phys. **9**, 709 (2013).
[10] V. Vildosola, F. Güller, and A. M. Llois, Phys. Rev. Lett. **110**, 206805 (2013).
[11] C. Franchini, G. Kresse, and R. Podloucky, Phys. Rev. Lett. **102**, 256402 (2009).
[12] K. Foyevtsova, A. Khazraie, I. Elfimov, and G. A. Sawatzky, Phys. Rev. B **91**, 121114 (2015).
[13] R. Zeyher and K. Kunc, Solid State Commun. **74**, 805 (1990).
[14] P. Blaha, K. Schwarz, P. Dufek, G. Vielsack, and W. Weber, Z. Naturforsch., A: Phys. Sci. **49**, 129132 (1994).
[15] A. I. Liechtenstein, I. I. Mazin, C. O. Rodriguez, O. Jepsen, O. K. Andersen, and M. Methfessel, Phys. Rev. B **44**, 5388 (1991).
[16] K. Kunc, R. Zeyher, A. Liechtenstein, M. Methfessel, and O. Andersen, Solid State Commun. **80**, 325 (1991).
[17] V. Meregalli and S. Y. Savrasov, Phys. Rev. B **57**, 14453 (1998).
[18] C. Franchini, A. Sanna, M. Marsman, and G. Kresse, Phys. Rev. B **81**, 085213 (2010).
[19] D. Korotin, V. Kukolev, A. V. Kozhevnikov, D. Novoselov, and V. I. Anisimov, J. Phys.: Condens. Matter **24**, 415603 (2012).
[20] T. Bazhirov, S. Coh, S. G. Louie, and M. L. Cohen, Phys. Rev. B **88**, 224509 (2013).
[21] Z. P. Yin, A. Kutepov, and G. Kotliar, Phys. Rev. X **3**, 021011 (2013).
[22] A. F. Kusmartseva, B. Sipos, H. Berger, L. Forró, and E. Tutiš, Phys. Rev. Lett. **103**, 236401 (2009).
[23] M. Leroux, I. Errea, M. Le Tacon, S.-M. Souliou, G. Garbarino, L. Cario, A. Bosak, F. Mauri, M. Calandra, and P. Rodière, Phys. Rev. B **92**, 140303 (2015).
[24] M. Hanfland, K. Syassen, N. Christensen, and D. Novikov, Nature (London) **408**, 174 (2000).
[25] Y. Ma, M. Eremets, A. R. Oganov, Y. Xie, I. Trojan, S. Medvedev, A. O. Lyakhov, M. Valle, and V. Prakapenka, Nature (London) **458**, 182 (2009).
[26] D. Duan, Y. Liu, F. Tian, D. Li, X. Huang, Z. Zhao, H. Yu, B. Liu, W. Tian, and T. Cui, Sci. Rep. **4**, 6968 (2014).
[27] A. P. Drozdov, M. I. Eremets, I. A. Troyan, V. Ksenofontov, and S. I. Shylin, Nature (London) **525**, 73 (2015).
[28] A. Drozdov, M. I. Eremets, and I. A. Troyan, arXiv:1508.06224.
[29] C. Heil and L. Boeri, Phys. Rev. B **92**, 060508 (2015).
[30] J. Flores-Livas, A. Sanna, and E. K. U. Gross, Eur. Phys. J. B **89**, 63 (2016).
[31] N. Bernstein, C. S. Hellberg, M. D. Johannes, I. I. Mazin, and M. J. Mehl, Phys. Rev. B **91**, 060511 (2015).
[32] I. Errea, M. Calandra, C. J. Pickard, J. Nelson, R. J. Needs, Y. Li, H. Liu, Y. Zhang, Y. Ma, and F. Mauri, Phys. Rev. Lett. **114**, 157004 (2015).
[33] J. A. Flores-Livas, M. Amsler, C. Heil, A. Sanna, L. Boeri, G. Profeta, C. Wolverton, S. Goedecker, and E. K. U. Gross, Phys. Rev. B **93**, 020508 (2016).
[34] A. Shamp, T. Terpstra, T. Bi, Z. Falls, P. Avery, and E. Zurek, J. Am. Chem. Soc. **138**, 1884 (2016).
[35] Y. Fu, X. Du, L. Zhang, F. Peng, M. Zhang, C. J. Pickard, R. J. Needs, D. J. Singh, W. Zheng, and Y. Ma, Chem. Mater. **28**, 1746 (2016).
[36] C. Kokail, C. Heil, and L. Boeri, Phys. Rev. B **94**, 060502 (2016).
[37] E. Wigner and H. Huntington, J. Chem. Phys. **3**, 764 (1935).
[38] P. Cudazzo, G. Profeta, A. Sanna, A. Floris, A. Continenza, S. Massidda, and E. K. U. Gross, Phys. Rev. Lett. **100**, 257001 (2008).
[39] M. Borinaga, I. Errea, M. Calandra, F. Mauri, and A. Bergara, Phys. Rev. B **93**, 174308 (2016).
[40] R. Dias and I. Silvera, Science **355**, 715 (2017).
[41] H. T. Stokes, D. M. Hatch, and J. D. Wells, Phys. Rev. B **43**, 11010 (1991).
[42] The ISOTROPY software suite is a collection of software which applies group-theoretical methods to the analysis of phase transitions in crystalline solids; see http://stokes.byu.edu/iso/isotropy.php.
[43] A. R. Oganov and C. W. Glass, J. Chem. Phys. **124**, 244704 (2006).
[44] H. T. Stokes, Introduction to Isotropy Subgroups and Displacive Phase Transitions (unpublished), http://stokes.byu.edu/iso/2006%20Stokes.pdf .
[45] J. Heyd, G. E. Scuseria, and M. Ernzerhof, J. Chem. Phys. **118**, 8207 (2003).
[46] R. Scholder, K.-W. Ganter, H. Gläser, and G. Merz, Z. Anorg. Allg. Chem. **319**, 375 (1963).
[47] T. Nakamura, S. Kose, and T. Sata, J. Phys. Soc. Jpn. **31**, 1284 (1971).
[48] R. Arpe and H. Müller-Buschbaum, Z. Anorg. Allg. Chem. **434**, 73 (1977).
[49] To model the effect of pressure on the system we performed a set of fixed-volume relaxations for different volume values allowing atomic positions and unit cell shape to vary. The corresponding pressure at each volume was obtained from the stress tensor.
[50] See Supplemental Material at http://link.aps.org/supplemental/10.1103/PhysRevB.96.035103 for CIF files of the ground-state structures.
[51] See Supplemental Material at http://link.aps.org/supplemental/10.1103/PhysRevB.96.035103 for the extended version of the phase diagram plot.
[52] A. R. Oganov and S. Ono, Nature (London) **430**, 445 (2004).
[53] H. Sugiura and T. Yamadaya, Solid State Commun. **49**, 499 (1984).
[54] H. Sugiura and T. Yamadaya, Physica B+C **139-140**, 349 (1986).
[55] C. J. Howard and H. T. Stokes, Acta Crystallogr., Sect. A **61**, 093 (2005).
[56] P. V. Balachandran and J. M. Rondinelli, Phys. Rev. B **88**, 054101 (2013).
[57] J. He and C. Franchini, Phys. Rev. B **89**, 045104 (2014).
[58] A. Togo and I. Tanaka, Scr. Mater. **108**, 1 (2015).
[59] PHONOPY website: https://atztogo.github.io/phonopy/. PHONOPY is a package for phonon calculations at harmonic and

quasiharmonic levels and uses the supercell approach with the finite displacements method. It finds the corresponding force constants, builds the dynamical matrix, diagonalizes it, and then calculates the phonon dispersion relaxations.

[60] See Supplemental Material at http://link.aps.org/supplemental/10.1103/PhysRevB.96.035103 for the plot of evolution with respect to pressure of the calculated phonon frequencies for selected irreducible representations for ideal cubic $BaBiO_3$.

[61] A. M. Glazer, Acta Crystallogr., Sect. A **31**, 756 (1975).

[62] See Supplemental Material at http://link.aps.org/supplemental/10.1103/PhysRevB.96.035103 for the description of the band gap, distortions, and charge difference evolution with respect to pressure for monoclinic $BaBiO_3$.

[63] See Supplemental Material at http://link.aps.org/supplemental/10.1103/PhysRevB.96.035103 for the table describing irreducible representations and order parameters used to obtain structures predicted using the phonon mode analysis method.

[64] S. P. Ong, W. D. Richards, A. Jain, G. Hautier, M. Kocher, S. Cholia, D. Gunter, V. L. Chevrier, K. A. Persson, and G. Ceder, Comput. Mater. Sci. **68**, 314 (2013).

[65] CHEMENV is a module inside the PYMATGEN package and is developed by David Waroquiers and Geoffroy Hautier. Website: http://pymatgen.org/.

[66] D. Waroquiers and G. Hautiers (private communication).

[67] PYMATGEN is a PYTHON programming language library for materials analysis that has capabilities for generation of phase diagrams, Pourbaix diagrams, diffusion analysis, reactions, electronic structure analysis, etc. Also, it provides tools to construct, manipulate, and analyze structures. One of them is the CHEMENV module that is developed for chemical environment analysis.

[68] See Supplemental Material at http://link.aps.org/supplemental/10.1103/PhysRevB.96.035103 for "D. Neighbors analysis" subsection.

[69] It is possible to precisely determine the difference of partial DOS only for monoclinic $C12\bar{m}1$ $BaBiO_3$ as it has only two Bi atoms which are inequivalent. For the other structures we have separated Bi atoms into two formal groups representing the Bi^{5+} and Bi^{3+} cases. After averaging the partial DOS in each group the difference was taken.

[70] Using the HSE functional on top of the $C12\bar{m}1^C$ obtained at the PBE level leads to a semimetal solution. We investigated this case further and performed structure optimization at HSE level for this structure; as a result the gap is opened. To be consistent with the data for other structures on the plot, we left PBE+HSE data for $C12\bar{m}1^C$ in Fig. 5.

[71] R. Martok, D. Ceresoli, T. Kagayama, Y. Matsuda, Y. Yamada, and E. Tosatti, Phys. Rev. Materials **1**, 023601 (2017).

[72] G. Kresse and J. Hafner, Phys. Rev. B **47**, 558 (1993).

[73] G. Kresse and J. Hafner, Phys. Rev. B **49**, 14251 (1994).

[74] G. Kresse and J. Furthmüller, Comput. Mater. Sci. **6**, 15 (1996).

[75] G. Kresse and J. Furthmüller, Phys. Rev. B **54**, 11169 (1996).

[76] G. Kresse and D. Joubert, Phys. Rev. B **59**, 1758 (1999).

[77] P. E. Blöchl, Phys. Rev. B **50**, 17953 (1994).

[78] H. J. Monkhorst and J. D. Pack, Phys. Rev. B **13**, 5188 (1976).

[79] J. D. Pack and H. J. Monkhorst, Phys. Rev. B **16**, 1748 (1977).

[80] J. P. Perdew, K. Burke, and M. Ernzerhof, Phys. Rev. Lett. **77**, 3865 (1996).

[81] J. P. Perdew, K. Burke, and M. Ernzerhof, Phys. Rev. Lett. **78**, 1396 (1997).

[82] See Supplemental Material at http://link.aps.org/supplemental/10.1103/PhysRevB.96.035103 for explanation of the chemical environment determination procedure.